
Optimizing High-Dimensional Physics Simulations via Composite Bayesian Optimization

Wesley J. Maddox*
New York University
wjm363@nyu.edu

Qing Feng
Facebook
qingfeng@fb.com

Max Balandat
Facebook
balandat@fb.com

Abstract

Physical simulation-based optimization is a common task in science and engineering. Many such simulations produce image- or tensor-based outputs where the desired objective is a function of those outputs, and optimization is performed over a high-dimensional parameter space. We develop a Bayesian optimization method leveraging tensor-based Gaussian process surrogates and trust region Bayesian optimization to effectively model the image outputs and to efficiently optimize these types of simulations, including a radio-frequency tower configuration problem and an optical design problem.

1 Introduction

Many design problems in the physical sciences require running simulations to evaluate a new design. Examples abound in material science (Zhang et al., 2020), fluid dynamics (Anderson and Wendt, 1995), and optics (O’Shea et al., 2004). Typically, these simulations generate high-dimensional outputs, often in the form of image- or other tensor-structured formats. This usually requires substantial computational effort and simulations may take a long time to run. Optimizing designs thus presents a formidable challenge, and using sample-efficient optimization methods is crucial.

In this work, we solve a challenging design problem, namely optimizing the geometry and gratings of a diffractive optical element. In our example the design is parameterized by 177 parameters; each simulation takes about one hour to run and produces an $11 \times 16 \times 16$ output representing the projected image. Our goal is to explore the efficient frontier between efficiency (how much light is delivered) and uniformity (how uniform is the output) of the image generated by the device.

One approach to optimizing such a problem is to build a surrogate model of the simulation that is cheap/quick to evaluate, and perform the optimization utilizing this surrogate. Bayesian Optimization (BO) is an established method following this paradigm, and has been successfully applied in wide range of settings, including many in the physical sciences (Packwood, 2017; Zhang et al., 2020; Duris et al., 2020). Historically, BO has been restricted to relatively low-dimensional design spaces, a small number of evaluations, and a single scalar outcome. Recently, Maddox et al. (2021a) developed a scalable approach to *composite* BO with high-dimensional outputs that relies on an efficient sampling scheme for High-Order Gaussian Process (HOGP) models that provide a probabilistic model over tensor-structured outputs. However, their method suffers from the same scaling challenges in terms of the dimension of the *design* space as standard GP models do (Eriksson et al., 2019; Eriksson and Poloczek, 2021), and is thus not applicable to our 177-dimensional optics optimization problem.

In this work, we combine the model and sampling scheme from Maddox et al. (2021a) with the recent MORBO algorithm for high-dimensional multi-objective Bayesian Optimization from Daulton et al. (2021). We overcome additional memory scalability challenges by employing a mixed-precision compute paradigm and batching computations, enabling improved performance over existing baselines.

*Work performed during an internship at Facebook.

2 Methodology

2.1 High-Order Gaussian Process for Image Pixel Prediction

To perform composite Bayesian Optimization in the space of large images, we use the high-order Gaussian Process (HOGP) proposed by Zhe et al. (2019) to model the images from the optics simulator given a design configuration. This model extends the traditional multi-task Gaussian processes (MTGPs) and can more efficiently handle high-dimensional correlated outputs.

The HOGP model tensorizes the image outputs $\mathbf{y} \in \mathbb{R}^{n \times d_1 \times \dots \times d_k}$, and learns latent features of each tensor element to capture their correlations. It assumes the covariance between any two outputs, \mathbf{y}, \mathbf{y}' , is given as the elementwise product of the output indices. The covariance function is

$$k([x, i_1, \dots, i_k], [x', j_1, \dots, j_k]) = k(x, x')k(v_1, v'_1) \dots k(v_k, v'_k),$$

where i_1, \dots, i_k are the indices for the output tensor, v_1, \dots, v_k are the latent parameters, and $k(x, x')$ is the kernel over the parameter space. Thus, the task covariance function in the MTGP framework is represented as a chain of Kronecker products so that the GP prior is $\text{vec}(\mathbf{y}) \sim \mathcal{N}(0, K_{XX} \otimes K_2 \otimes \dots \otimes K_k)$. See Appendix B.1 for more discussions.

2.2 Composite Multi-objective Optimization over High-dimensional Search Space

Given the images predicted from the HOGP model, we can perform composite BO (Astudillo and Frazier, 2019) that optimizes composite objectives of the form $\max_x g(h(x))$, where $h : \mathbb{R}^d \rightarrow \mathbb{R}^{d_1 \times \dots \times d_k}$ is the expensive simulation that produces a tensor as output, and $g : \mathbb{R}^{d_1 \times \dots \times d_k} \rightarrow \mathbb{R}^o$ is the deterministic function to compute goal metric e.g. efficiency of image outputs.

The optical design problem poses two primary challenges: 1) the design space is high-dimensional with 177 parameters to optimize; 2) the goal is to find the set of optimal tradeoffs between the two competing objectives (efficiency and uniformity) rather than optimizing a single objective. GP-based BO usually works well for problems with search spaces having less than 20 or so parameters, but does not scale well to high-dimensional parameter spaces: as distances grow larger and model uncertainty towards the boundary of the search space increases, BO tends to over-explore. To avoid this issue, Eriksson et al. (2019) introduced trust region Bayesian optimization (TRBO) that performs optimization in smaller trust regions that evolve across the search space. More recently, (MORBO) Daulton et al. (2021) extended this work to the multi-objective setting. While MORBO handles high-dimensional *parameter* spaces well, Daulton et al. (2021) only considered problems with few outcomes and non-composite settings. In this work we employ MORBO in conjunction with the improved HOGP model to perform composite BO over high-dimensional *outcome* spaces (images).

2.3 Efficient Posterior Sampling for MORBO with HOGP

MORBO/TRBO construct trust regions and perform local modeling and optimization. Thus, we build a HOGP using observations inside each trust region. Since the HOGP is a sample-efficient model, we can achieve good predictions of image pixels and the aggregated goal metrics (see Figure 4a for an example), and also reduce computational cost of using all the data points.

Both MORBO and TRBO rely on Thompson sampling for optimizing acquisition functions, which is typically implemented as drawing a large numbers of GP posterior samples evaluated at many discrete candidates, x_{test} . Drawing posterior samples from HOGPs can be computationally expensive and even be intractable for high-dimensional outputs such as images. The time complexity to naively sample over all outputs (tasks) and all new data points is multiplicative in the number of outputs $\mathcal{O}((n^3 + n_{\text{test}}^3) \prod_{i=1}^d d_i^3)$ (Maddox et al., 2021a). What's more, storing k posterior samples at n_{test} test points requires storage of $k \times n_{\text{test}} \times n \times d_1 \times \dots \times d_k$ tensors, which quickly becomes problematic on a memory-restricted GPU. To make it feasible to combine HOGP with MORBO/TRBO, we leverage the efficient posterior sampling developed by Maddox et al. (2021a) to reduce the time complexity to $\mathcal{O}((n^3 + n_{\text{test}}^3) + \sum_{i=1}^d d_i^3)$ (see Appendix B.2 for additional technical details) and further propose two remedies to improve memory complexity of posterior sampling.

First, we segment test points into smaller batches and loop batches of $n' \ll n_{\text{test}}$ test points, as they affect the size of the Kronecker matrix vector multiplications more than the number posterior samples, k . This results in smaller matrix vector products and thus reduced memory overheads. While this is

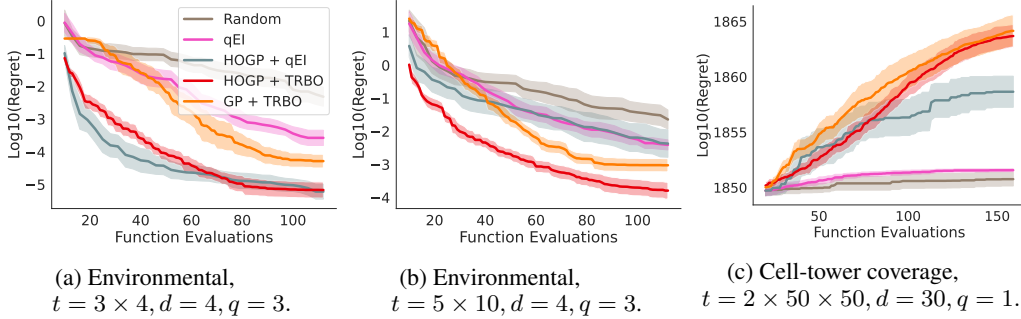


Figure 1: Benchmark traces (average across 20 runs with 95% confidence interval) for single objective problems. HOGP+TRBO achieves the best performance on the environmental problems and performs similarly as TRBO, obtaining the best reward on the cell-tower coverage problem.

not quite Thompson sampling due to the conditional independence between batches, we found that it does not empirically lead to a large degradation in performance. However, we hope to improve on this strategy in future work.

Second, we employ a mixed-precision computing paradigm and use half precision arithmetic to compute the Kronecker matrix vector products when evaluating the posterior samples, while using double precision for the numerically demanding matrix root computation of the potentially poorly conditioned data covariance. Unlike previous work such as Gardner et al. (2018); Maddox et al. (2021b) that found implementation difficulties when moving to lower precision arithmetic, we perform all training in float and double precision arithmetic, and only compute the posterior Kronecker matrix vector products (which are the memory intensive ones) in half precision. This enables accurate computations when necessary, while preserving much of the speedups gained by using lower precision arithmetic (Mickevičius et al., 2017).

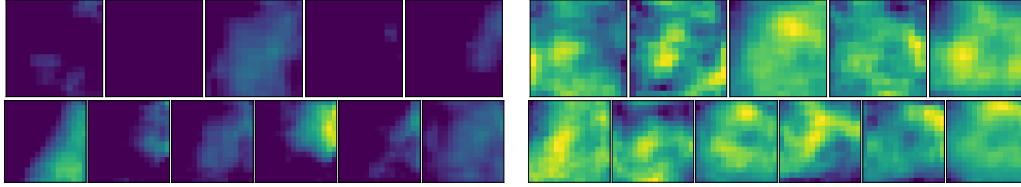
3 Results and Discussion

3.1 Single Objective Experiments

We evaluate our method (HOGP+TRBO) that performs composite TRBO with HOGP model on three single objective optimization problems, and compare with four methods: quasi-random search (Random), expected improvement on the metric (qEI), current TRBO (GP+TRBO) and composite BO with HOGP and expected improvement (HOGP+EI). All the results are the mean and 95% confidence intervals across 20 trials. See Appendix C.1 for additional experimental details.

Environmental Problem We evaluate on a spatial problem in which environmental pollutant concentrations are observed on a 3×4 grid originally defined in Bliznyuk et al. (2008); Astudillo and Frazier (2019) and an expanded 5×10 grid. The goal is to optimize a set of four parameters to achieve the true observed value by minimizing the mean squared error of the output grid to the output grid of the true parameters. As shown in Figure 1a and Figure 1b, current TRBO achieves lower regret compared with Random and qEI and our method further outperforms TRBO. This demonstrates the efficiency of performing composite Bayesian optimization with HOGP.

Cell-Tower Coverage Problem Following Maddox et al. (2021a); Dreifuerst et al. (2020), we optimize the simulated “coverage map” resulting from the transmission power and down-tilt settings of 15 cell towers (for a total of 30 parameters) based on a scalarized quality metric combining signal power and interference at each location so as to maximize total coverage, while minimizing total interference. To reduce model complexity, we down-sample the simulator output to 50×50 , initializing the optimization with 20 random configurations. Figure 1c shows that our method and current TRBO achieve the best performance.



(a) Example image outputs from simulations. (b) Example optimized image outputs from simulations.

Figure 2: Example output images (un-optimized (a) and optimized (b) using our approach (HOGP+MORBO) on the diffractive optical element problem; pixel values are displayed on the same scale per panel. The ideal output would be uniformly bright images. The optimized channels are significantly brighter and are smoother at same time as would be expected from optimizing both the efficiency and uniformity metrics.

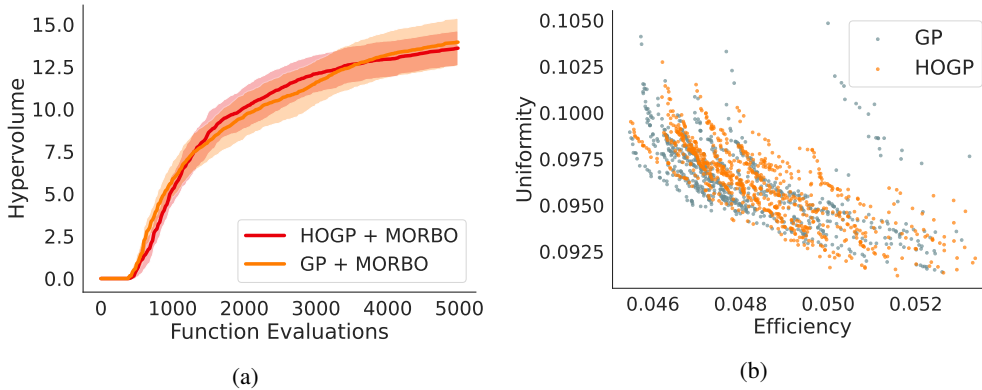


Figure 3: Performance on the multi-objective optical design problem. (a) HOGP+MORBO outperforms GP+MORBO in the early iterations and achieves similar maximum hypervolume at the end. (b) Pareto frontiers (metrics are standardized so that lower is better for both metrics) over 20 trials. HOGP+MORBO can push more on optimizing uniformity which is harder to model.

3.2 Multi-Objective Design of a Diffractive Optical Element

We compare our multi-objective optimization approach (HOGP+MORBO) with current MORBO (GP+MORBO) (Daulton et al., 2021) on the 177-dimensional optics optimization problem. The simulations generating the outputs of the elements are computed using a custom physics simulation engine. In order to evaluate the optimization performance at reasonable computational cost, we fit a neural network surrogate model from the input parameterization to the image output based on a large number of simulation runs sampled from the design space. In the benchmarks, we evaluate designs based on this neural network surrogate rather than the real physics simulation engine. See Appendix C.2 for the details of optical experimental setup. The goal is to jointly minimize two goal metrics, efficiency and uniformity, used for measuring displayed image quality. We assess the performance based on the maximum achieved hyper-volume.

Figure 2b demonstrates the substantial improvements on the displayed images through optimizing with HOGP+MORBO. The optimized images are much brighter and are also smoother compared to the un-optimized outputs. Figure 3a shows that our approach tends to outperform current MORBO in the earlier stage of the optimization and reaches to a similar performance at the end. We further visualize the Pareto frontiers (metrics are standardized) across 20 runs in Figure 3b. It can be seen that the HOGP can explore along the uniformity metric more efficiently than the GP model, but explores less on the efficiency metric. Since the uniformity metric (defined as a ratio between extreme pixel values) is a harder to model than efficiency (which is closely related to the average pixel brightness), this again suggests the sample efficiency of HOGP from modeling the image outputs directly and learning the latent correlation structure across image pixels to transfer information.

Acknowledgements

WJM was partially supported by a NSF Graduate Research Fellowship under NSF IIS-1951856. We'd like to thank Dominic Meiser, Ningfeng Huang, Eytan Bakshy, and David Eriksson.

References

- Anderson, J. D. and Wendt, J. (1995). *Computational fluid dynamics*, volume 206. Springer.
- Astudillo, R. and Frazier, P. (2019). Bayesian Optimization of Composite Functions. In *International Conference on Machine Learning*, pages 354–363. PMLR. ISSN: 2640-3498.
- Balandat, M., Karrer, B., Jiang, D., Daulton, S., Letham, B., Wilson, A. G., and Bakshy, E. (2020). BoTorch: A Framework for Efficient Monte-Carlo Bayesian Optimization. In *Advances in Neural Information Processing Systems*, volume 33.
- Bliznyuk, N., Ruppert, D., Shoemaker, C., Regis, R., Wild, S., and Mugunthan, P. (2008). Bayesian calibration and uncertainty analysis for computationally expensive models using optimization and radial basis function approximation. *Journal of Computational and Graphical Statistics*, 17(2):270–294.
- Daulton, S., Eriksson, D., and Balandat, M. (2021). Multi-objective bayesian optimization over high-dimensional search spaces. *arXiv preprint arXiv:2109.10964*.
- Dreifuerst, R. M., Daulton, S., Qian, Y., Varkey, P., Balandat, M., Kasturia, S., Tomar, A., Yazdan, A., Ponnampalam, V., and Heath, R. W. (2020). Optimizing coverage and capacity in cellular networks using machine learning. *arXiv preprint arXiv:2010.13710*.
- Duris, J., Kennedy, D., Hanuka, A., Shtalenkova, J., Edelen, A., Baxevanis, P., Egger, A., Cope, T., McIntire, M., Ermon, S., and Ratner, D. (2020). Bayesian optimization of a free-electron laser. *Phys. Rev. Lett.*, 124:124801.
- Eriksson, D., Pearce, M., Gardner, J., Turner, R. D., and Poloczek, M. (2019). Scalable global optimization via local bayesian optimization. *Advances in Neural Information Processing Systems*, 32:5496–5507.
- Eriksson, D. and Poloczek, M. (2021). Scalable constrained bayesian optimization. In *International Conference on Artificial Intelligence and Statistics*. PMLR.
- Gardner, J., Pleiss, G., Weinberger, K. Q., Bindel, D., and Wilson, A. G. (2018). GPyTorch: Blackbox Matrix-Matrix Gaussian Process Inference with GPU Acceleration. In *Advances in Neural Information Processing Systems*, volume 31, pages 7576–7586.
- Goovaerts, P. et al. (1997). *Geostatistics for natural resources evaluation*. Oxford University Press on Demand.
- Maddox, W. J., Balandat, M., Wilson, A. G., and Bakshy, E. (2021a). Bayesian optimization with high-dimensional outputs. *arXiv preprint arXiv:2106.12997*.
- Maddox, W. J., Kapoor, S., and Wilson, A. G. (2021b). When are iterative gaussian processes reliably accurate? In *OPTML Workshop at International Conference on Machine Learning (ICML)*.
- Micikevicius, P., Narang, S., Alben, J., Damos, G., Elsen, E., Garcia, D., Ginsburg, B., Houston, M., Kuchaiev, O., Venkatesh, G., et al. (2017). Mixed precision training. *arXiv preprint arXiv:1710.03740*.
- O’Shea, D. C., Suleski, T. J., Kathman, A. D., and Prather, D. W. (2004). *Diffraction optics: design, fabrication, and test*, volume 62. SPIE press.
- Packwood, D. (2017). *Bayesian Optimization for Materials Science*. Springer.
- Rasmussen, C. E. and Williams, C. K. I. (2008). *Gaussian processes for machine learning*. Adaptive computation and machine learning. MIT Press, Cambridge, Mass., 3. print edition.

Zhang, Y., Apley, D. W., and Chen, W. (2020). Bayesian optimization for materials design with mixed quantitative and qualitative variables. *Scientific reports*, 10(1):1–13.

Zhe, S., Xing, W., and Kirby, R. M. (2019). Scalable High-Order Gaussian Process Regression. In *The 22nd International Conference on Artificial Intelligence and Statistics*, pages 2611–2620. PMLR. ISSN: 2640-3498.

A Broader Impact Statement

The method introduced in this paper provides a sample-efficient solution to the challenging design problems in the physical sciences. By overcoming the scalability blockers in leveraging tensor-based Gaussian Process model and trust region Bayesian Optimization, we unlock the possibilities of conducting optimizations in high-dimensional parameter spaces and output spaces. We do not expect any negative social impacts from our work.

B Methodological Details

B.1 Kronecker Matrix Vector Products

The key aspect of efficiency in the HOGP comes from *Kronecker matrix vector products*. Such structure allows it to capture complex output correlations and scale to high-dimensional outputs with no sparse approximation. Besides, kronecker matrix vector multiplies (MVMs) can be efficiently computed from:

$$z = (K_1 \otimes K_2)\text{vec}(A) = \text{vec}(K_2AK_1^\top);$$

if $K_1 \in \mathbb{R}^{n_1 \times n_1}$ and $K_2 \in \mathbb{R}^{n_2 \times n_2}$. As a result, computing z costs $\mathcal{O}(n_1^2 + n_2^2 + n_1n_2(n_1 + n_2))$ time. Note that we can recursively compute this structure across several matrix vector products. Implementation wise, this involves reshaping the vector $\text{vec}A$ to be a matrix and then computing a matrix matrix product, for example K_2A .

B.2 Efficient Posterior Sampling with the HOGP

We utilize the efficient posterior sampling mechanism for the HOGP model Maddox et al. (2021a) proposes an efficient posterior sampling mechanism for general MTGPs and extends it to HOGPs as a special case. The time complexity of this method is additive in the combination of tasks and data points, rather than multiplicative, which allows us to perform time-efficient composite Bayesian Optimization on the image outputs.

This method uses Matheron’s rule for sampling conditional Gaussian distributions (Goovaerts et al., 1997). For HOGP, $f(x_{\text{test}})|Y = y$ generated by Matheron’s rule can be represented as

$$\bar{f} = f + (K_{x_{\text{test}}X} \otimes_{i=2}^d K_i) \left((K_{XX} \otimes_{i=2}^d K_i) + \sigma^2 I \right)^{-1} (y - Y - \epsilon), \quad (1)$$

where $f \sim \mathcal{N}(0, K_{(x_{\text{test}}, X), (x_{\text{test}}, X)} \otimes_{i=2}^d K_i)$, that is drawn from the joint prior distribution that all kernel matrices are Kronecker structured, and $\epsilon \sim \mathcal{N}(0, \sigma^2 I)$. Although the size of \bar{f} is still $\sum_{i=1}^k d_i$ and naively decomposing the posterior covariance matrix of the GP to produce posterior samples would cost $\mathcal{O}((\sum_{i=1}^k d_i)^3)$ time, the Matheron’s rule approach instead costs $\mathcal{O}(\sum_{i=1}^k d_i^3 + \sum_{i=1}^k d_i)$ time to draw a single sample.

C Experimental Details

C.1 Single Objective Experimental Details

In the benchmarks, the HOGP model and TRBO used reference implementations from their authors with default settings. For qEI and GP+TRBO, we used a standard ARD Matern 5/2 kernel (Rasmussen and Williams, 2008) to model the aggregated goal metrics. For the methods using expected improvement, we used the *qExpectedImprovement* acquisition implemented in BoTorch (Balandat et al., 2020).

For the environmental problem, we followed the implementations of Balandat et al. (2020), Astudillo and Frazier (2019), and used 8 random restarts, 256 MC samples, and 512 base samples, a batch limit of 4, and an initialization batch limit of 8.

For the radio frequency coverage problem, we followed the evaluation setup in Maddox et al. (2021a). We initialized with 20 points, down-sampled the two 241×241 outputs to 50×50 for simplicity, ran the experiments over 20 random seeds and for 150 steps. We used 32 MC samples, 64 raw samples with a batch limit of 4 and an initialization batch limit of 16.

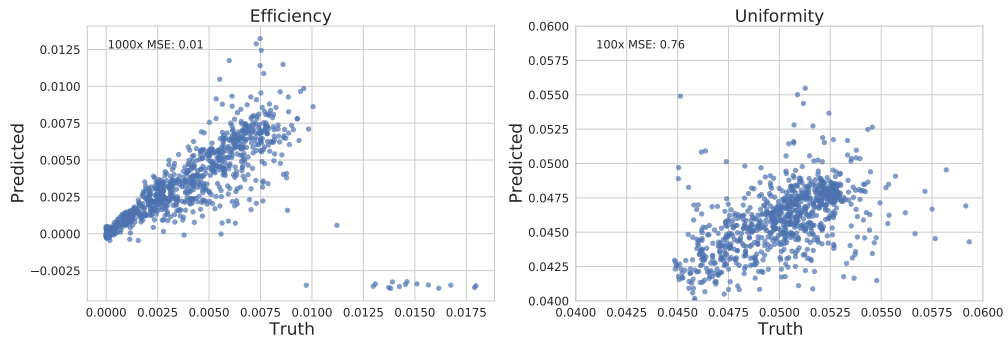
C.2 Diffractive Optical Element Design

The surrogate model is a densenet style architecture and maps the 177 dimensional input parameters into the 11 output images, each of which is of size 16×16 . Example images that are optimized are shown in Figure 2a. The goal of these design efforts is to jointly optimize the efficiency and uniformity of the images. Efficiency is computed as a weighted mean across an images, while uniformity is computed as a ratio of the 99% percentile pixel in the image to the 1% percentile pixel in the image. To combine the metrics across images, we consider the log sum exp of all of the images as a form of soft maximum.² As the real simulation itself is noisy, we use a scale Binomial noise term to inject noise into the image after being outputted from the surrogate NN model: each image pixel is drawn from a distribution following $y \sim \text{Binomial}(N, p * 100) / (100 * N)$, where $N = 5000$. This type of noise model matches the underlying physical structure of the simulator.

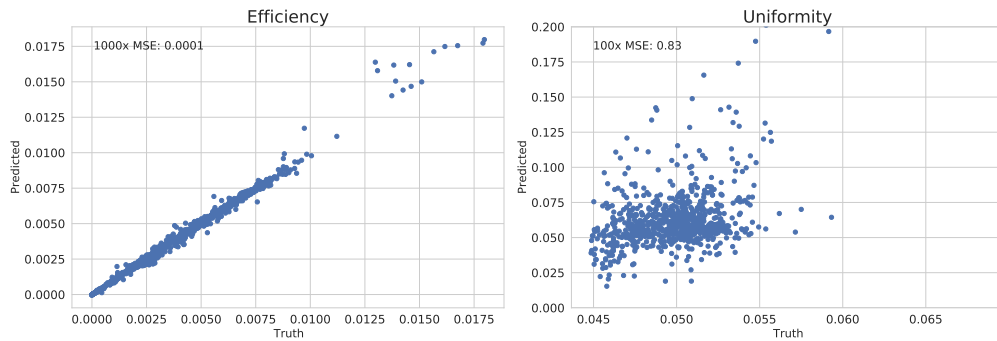
Experimental Details We used the MORBO implementation as referenced in Daulton et al. (2021). Each trial was initialized with 400 Sobol points and optimized the hypervolume improvement with batch sizes of 50 over 5000 function evaluations. The results shown in Figure 3a are the mean and 95% confidence intervals (2 standard errors) of the achieved maximum hyper-volume across 20 trials.

Benchmark Result Analysis We evaluate the out-of-sample prediction accuracy of standard GP and HOGP model shown in Figures 4a and 4b. The plots compare the prediction of two goal metrics on a holdout set of data from an optimization run. We see that while both models are reasonably accurate at predicting both metrics, the GP is more accurate at predicting the efficiency metric, explaining why it was able to explore across the Pareto frontier better on that metric. By comparison, the HOGP is able to use the information of all pixels to better predict the uniformity metric, which is tougher to model and more bi-modal — we truncated the test set to remove the outliers.

²Please note that all scales of metrics in plots are normalized to be approximately $[0, 1]$.



(a) HOGP model fits on metrics after 5000 trials.



(b) GP model fits on metrics after 5000 trials.

Figure 4: Global surrogate model fits on the optics problem at the end of an optimization run (test / train sets are the same for both models). The GP surrogate is better at modelling efficiency, but is worse at modelling uniformity. The uniformity metric requires information across all pixels to be modelled accurately, so the HOGP is a better surrogate as it models each pixel.